2023-08-01

Density Functional Theory Study of Dopant Incorporation into Gamma-UO3

Nicholas James Wilson
University of Texas at El Paso

DENSITY FUNCTIONAL THEORY STUDY OF DOPANT

INCORPORATION INTO GAMMA-UO_3

NICHOLAS JAMES WILSON

Master's Program in Physics

APPROVED:

____
Eunja Kim, Ph.D., Chair

____
Mark R. Pederson, Ph.D.

____
James D. Kubicki, Ph.D.

____
Stephen L. Crites, Jr., Ph.D.
Dean of the Graduate School

DENSITY FUNCTIONAL THEORY STUDY OF DOPANT

INCORPORATION INTO GAMMA-UO_3

by

NICHOLAS JAMES WILSON, B.S.

THESIS

Presented to the Faculty of the Graduate School of

The University of Texas at El Paso

in Partial Fulfillment

of the Requirements

for the Degree of

MASTER OF SCIENCE

Department of Physics

THE UNIVERSITY OF TEXAS AT EL PASO

August 2023

Acknowledgments

I would first like to express my immense gratitude to my advisor, Dr. Eunja Kim, without whose constant encouragement and guidance I would not have continued my studies beyond the undergraduate level. She has been an invaluable source of knowledge, support, and patience necessary for me to reach this point of my educational career. I would also like to thank my lab mates and friends, Daisy Lopez, Carlos Hernandez, Monica Herrera, and formerly Todd Lombardi, for providing insight and inspiration along the way. Special thanks for this work in particular go to Ashley Shields and Tyler Spano of Oak Ridge National Lab for spearheading the project and allowing me to join them on the journey, as well as Eduardo Montoya of the University of Nevada – Las Vegas whose parallel work on this project has helped this thesis come to fruition in a timely manner. I would also like to acknowledge my committee members, Dr. Mark Pederson and Dr. James Kubicki, for their time and consideration in support and review of my work.

Outside the university, I would like to thank my parents and my brother for their love and support in all my pursuits, both personal and professional. I also want to thank Teresa, Jakoby, Vincent, and all my other friends for being pillars of companionship and comfort in this challenging endeavor. And, finally, to Odalys for his endless devotion and encouragement at the conclusion of this leg of my educational journey.

Funding for this work was provided by the National Nuclear Security Administration, Office of Defense Nuclear Nonproliferation, and partial support received from the DOE Office of Nuclear Energy's Nuclear Energy University Program (NEUP).

Abstract

Uranium trioxide (UO_3) is a stable uranium oxide found throughout the nuclear fuel cycle. The γ-UO_3 phase is of particular interest as the most stable at ambient conditions. As such, the γ-UO_3 structure was selected for a theoretical investigation into the incorporation of metal dopants for nuclear intentional forensics applications. The two lattice types of this phase, tetragonal ($I4_1/amd$) and orthorhombic (Fddd), were investigated and found to be energetically identical, and as such the smaller tetragonal structure was selected for doping. Three transition metal dopants (Cr, Fe, and Ni) were incorporated into the structure interstitially and substitutionally at a total of six different sites. The most energetically favorable of these were investigated further through analysis of lattice parameters, bond distances, X-ray diffraction (XRD) patterns, and densities of states (DOS). These analyses led to the conclusions that interstitial doping of these three transition metals is much more energetically favorable than substitutional doping, and that Cr is the most likely candidate overall with a negative value for its defect formation energy.

Table of Contents

List of Tables

List of Figures

Chapter 1:
Introduction

1.1 Uranium Oxides

Uranium oxides are an essential part of the nuclear fuel cycle. There are many stable forms of these uranium oxygen systems, though much research has been focused on uranium dioxide (UO_2) due to its function as the primary nuclear fuel [1]–[3]. However, other higher uranium oxides are commonly encountered such as triuranium octoxide (U_3O_8) and uranium trioxide (UO_3) which can be interesting topics of study. Each of these forms has a role to play in the overall cycle of nuclear fuel. U_3O_8 is among the most stable oxide forms in the long-term and therefore quite favorable as an option for storage of spent nuclear fuel. UO_3 is a very common intermediary oxide in the fuel cycle, being the oxidized form of the U_3O_8 which is mined as ore. It is also interesting to note that the uranyl nitrate which comes from the dissolution of spent nuclear fuel rods can then be reheated directly into UO_3 for reprocessing purposes, meaning that UO_3 has an important role at both beginning and end of the nuclear fuel cycle [4]. Once in the form of UO_3, the uranium can then be reduced into its useful form of UO_2 by the simple addition of hydrogen gas [5].

1.2 Intentional Forensics

This study was carried out to analyze doping of the γ-UO_3 structure, selected as a representative early and late fuel cycle material for intentional forensics applications. Nuclear forensics is the process of identifying the origins of nuclear material when it is found outside typical regulated environments [6][7]. As nuclear material has such potential for misuse, study into nuclear forensics has steadily increased in priority. Uranium ore itself is among the most common targets for forensic analysis, as particular mineral deposits tend to leave signatures and impurities which can be used to uniquely locate the source of the ore, even as it is processed into the latter stages of the nuclear fuel cycle. Intentional forensics is therefore the practice of *deliberately* adding defect materials which can be quickly detected and analyzed in order to trace the origin of a given sample. This can be achieved through the addition of taggant (or, synonymously, dopant) materials into the matrix of the material itself. In the nuclear fuel cycle, a given unique taggant would ideally be identifiable at various stages in order to easily determine the origin and intended purpose of the material. This ease of detection and uniqueness allows taggants to function similarly to barcodes in forensic analysis – far simpler to use than existing mineral markers or other forensic tools.

1.3 Selection of Materials

1.3.1 Metal Taggants

Ideal taggants would be elements that are not naturally found in the original nuclear material, or even deliberately altered isotopes that could rapidly be identified and referenced in order to determine the origin of misplaced material and where along its cycle it may have diverged from its intent [8]. Thus, transition metals with many isotopes available become an ideal starting point[9]. In addition to being easily detectable, taggants should be inert so as not to affect the performance of highly regulated nuclear material in the fuel cycle. The taggants should also be able to remain distinct and detectable throughout the various stages of irradiation and refinement that nuclear material must undergo. A short list of elements may fit these requirements, but the focus for this study will be on chromium, nickel, and iron. These elements are isotopically diverse, able to withstand the high temperatures required for the creation of nuclear fuel pellets, and have small enough cross-sections so as not to interfere with fission reactions. With these three elements in mind, the goal of this work is ultimately to determine the ease of incorporating the taggants into the structure of the γ-UO_3 cell. Through DFT analysis, the energetic favorability can be compared between the three elements and their respective incorporation sites. The effects on the lattice structure of this taggant incorporation can be determined, with the total volume and bond distances surrounding the taggant being considered as well.

1.3.2 Uranium Trioxide

There are several polymorphs of UO_3 that have been confirmed to exist, including α, β, γ, δ, ε, and η, along with an amorphous phase [10]. The most stable polymorph of UO_3 at ambient conditions is γ-UO_3, which is also among the most often encountered phases. For these reasons this study is focused around γ-UO_3, though a parallel study is being conducted at time of publication focused on β-UO_3[11]. Within the γ-UO_3 polymorph, two lattice structures have been reported at differing temperatures: an orthorhombic structure (Fddd, space group 70), and a tetragonal structure ($I4_1$/amd, space group 141) [12]. A DFT comparison of these two structures was carried out as part of this study, with initial structures provided by Shields et al. [10]. The two structures were found to be very similar. The orthorhombic structure, as seen in Figure 1(a), is nearly exactly twice the size of the tetragonal structure, Figure 1(b), with twice the atoms. Optimized energy per formula unit (F.U.), as shown in Table 1, are identical between the two.

Table 1: Parameters of Orthorhombic and Tetragonal γ-UO_3

Space Group	Method	Lattice Parameters				V ($Å^3$/F.U.)	Total Energy (eV/F.U.)
		a (Å)	*b* (Å)	*c* (Å)	*α* (°)		
Fddd	DFT	9.86	20.17	9.81	90	975.52	-569.85
	Expt. [13]	9.79	19.93	9.71	90	956.96	-
$I4_1$/amd	DFT	6.96	6.96	20.21	90	978.88	-569.85
	Expt. [13]	6.90	6.90	19.98	90	951.20	-

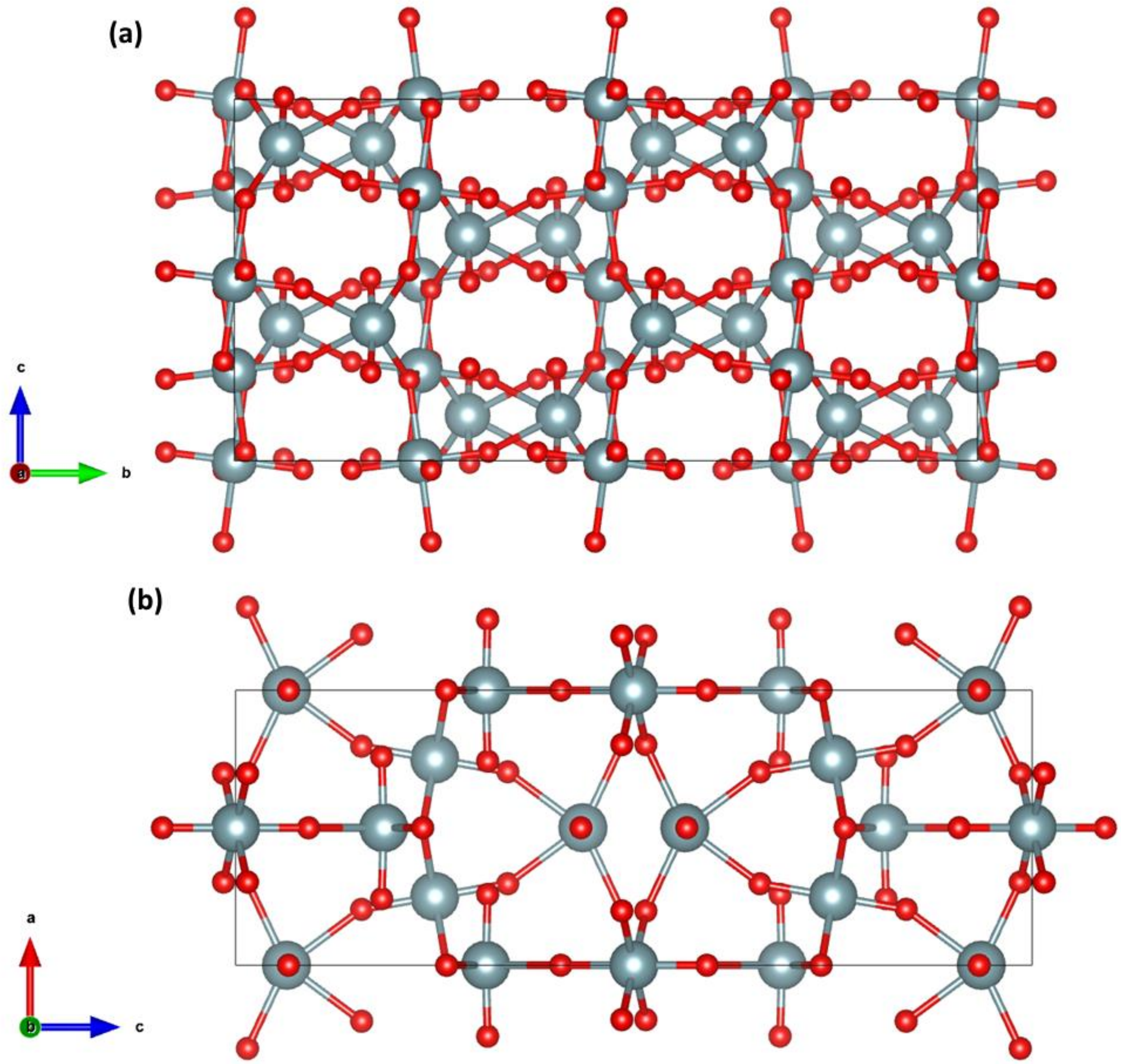

Figure 1: γ-UO_3: (a) Orthorhombic Fddd structure, (b) Tetragonal $I4_1/amd$ structure

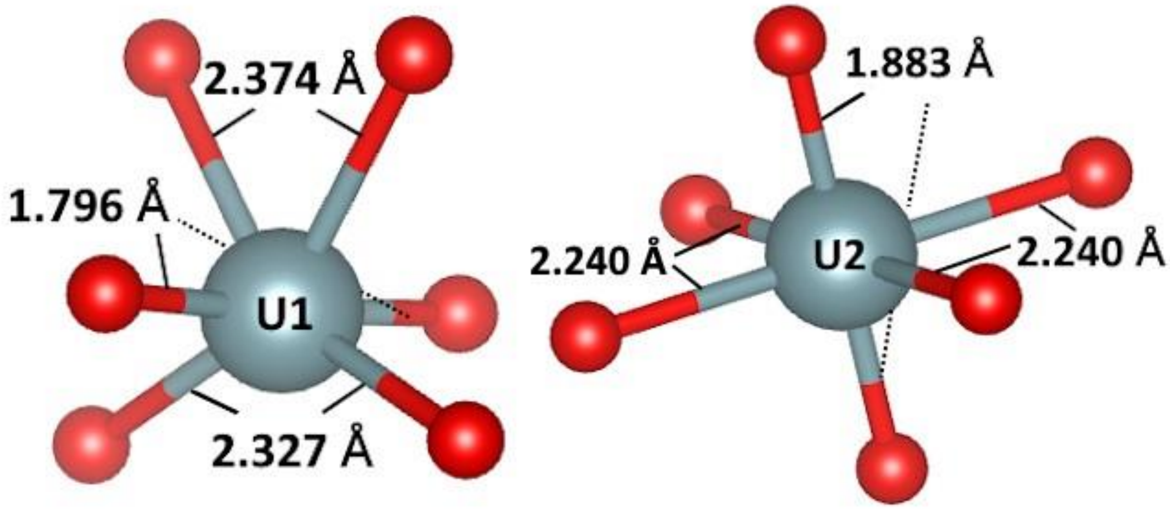

Figure 2: U-O bond distances for the two symmetrical U sites in γ-UO_3

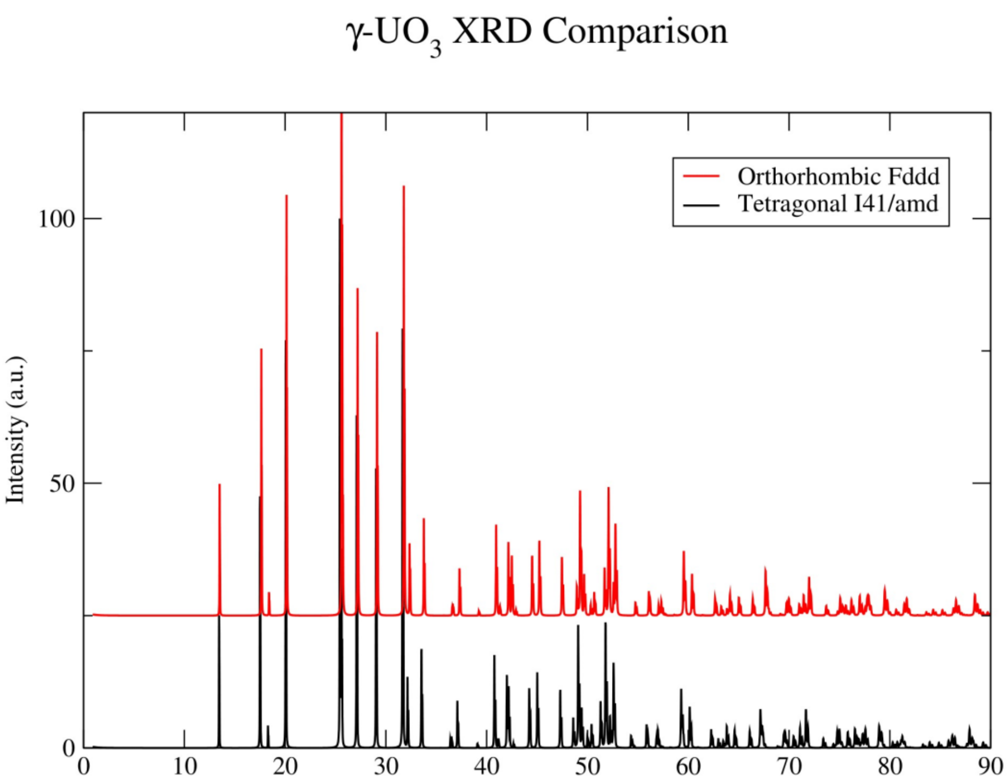

Figure 3: XRD pattern comparison for Orthorhombic and Tetragonal γ-UO_3 structures

Bond distances from the two U sites were also found to be identical between the two structures, with values for both U sites displayed in Figure 2. Compared with experimental values from Loopstra et al., DFT values show an approximate 2% overestimation in volume for both structures[13]. X-ray diffraction patterns for the two structures are also remarkably similar, as seen in Figure 3. The near-identical nature and symmetries of these two structures have shown their properties to be indistinguishable for the purposes of this study. As such, all calculations from this point were performed exclusively on the smaller tetragonal $I4_1$ structure for efficient use of computational resources.

Chapter 2:
Theoretical Methods

2.1 Density Functional Theory Calculations

Density functional theory (DFT) calculations in this study were performed using the Vienna Ab initio Simulation Package (VASP) along with the generalized gradient approximation (GGA) implemented within [14]–[17]. The standard Perdew-Burke-Ernzerhof (PBE) exchange-correlation functional was utilized for all calculations [18]. A plane wave basis set with an energy cutoff of 500 eV was used along with a Γ-centered *k*-points mesh of 3x3x3 for most calculations. Previous work from Brincat et al. on UO_3 structures found GGA+U corrections beneficial to correct for the strong correlation of the 5f electrons of uranium [19]. As such, the Dudarev method [20] for Hubbard correction was utilized, with a single parameter U_{eff} value of 3 eV for all uranium oxide calculations, like other past studies on similar materials [21][22][23]. For all structural calculations, unconstrained volume and lattice relaxations were carried out, and the resulting figures were modeled using VESTA [24]. X-ray diffraction (XRD) patterns were created using XMGRACE[25], and density of states (DOS) plots were generated using the Sumo package[26].

2.2 Doping Methodology

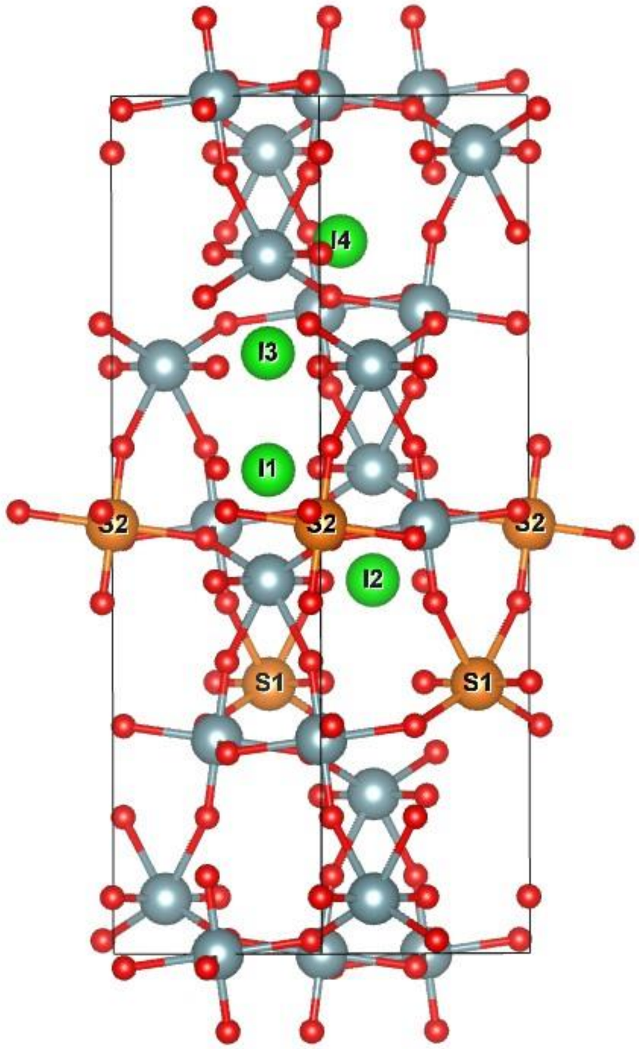

Figure 4: Tetragonal γ-UO_3 structure with labeled taggant incorporation sites. Red: O, Gray: U, Orange: Substitution, Green: Interstitial.

The main goal of this study was to understand the effect of incorporating particular transition metal taggants into the structure of the γ-UO_3 cell. As such, a uniform network of doping sites was employed to maintain consistency between the various structures. Symmetry calculations were carried out using the Phonopy package [27]. These symmetry considerations revealed that the γ-UO_3 structure consisted of a repeating arrangement of only two separate U^{6+} sites with three total symmetrically inequivalent O sites surrounding each. As such, these two U sites were determined to be sufficient for substitutional doping of the three candidate transition metals. The two substitution sites are the orange sites labeled *S1* and *S2* in Figure 4. Four additional interstitial sites were dispersed around the unit cell. These interstitial sites are the green sites labeled *I1-I4* in Figure 4. For each of the three transition metal taggants, all six of the substitutional and interstitial incorporation sites were introduced one at a time and allowed to relax positionally. The energetic results of these calculations form the core basis for eventual taggant favorability and selection.

2.3 Defect Formation Energy Calculation

In most DFT calculations, energetic outputs are typically used as the point of comparison between different structures. Energy minimization is the process of relaxing the positions of atoms such that their inter-atomic force is close to zero, and as such assumed to be in their lowest energy state. This means that the lower the total energy reported after the DFT calculations have concluded, the more favorable the formation of a given structure will be. These comparisons are straightforward between different incorporation sites of the same dopant in the same structure of γ-UO_3. However, when comparing the energies of different metal-doped structures or between interstitial and substitutional defect structures, these comparisons cannot be carried out directly. It is in these situations that a new parameter is required, known as the defect formation energy. An example of the calculation for the defect formation energy of interstitial Cr doping begins as follows:

$$16UO_3 + Cr \rightarrow Cr{:}\,16UO_3 \tag{1}$$

For this example, individual energy minimization calculations were carried out for the tetragonal UO_3 structure alone, as well as for the case of one Cr atom. When added together, these two values should create a corresponding "expectation value" for the energy of a single-dopant Cr:UO_3 structure. When this expectation energy is compared to the actual minimized energy given by DFT, a value for the defect formation energy is extracted. A similar process can be carried out for a substitutional taggant, with the caveat that the energy of the substitutionally replaced U atom must be removed from consideration in the expectation value, as in the chemical equation:

$$U_{16}O_{48} + Cr \rightarrow U_{15}O_{48}Cr + U \tag{2}$$

While the necessary calculations for interstitial and substitutional defect formation energies are different, the process results in a single, directly comparable value between all taggant incorporation methods, meaning that the most favorable structure overall between the six defect sites can be found. This same process can be generalized to the other taggant metals as well, since the individual metal is being corrected for in the defect formation energy calculation. This means that energetics can be compared between each of the defect types and each of the metal taggants, allowing for the selection of the most favorable structure from among all performed calculations and thus the best taggant candidate overall. To note, by this method of calculation a lower value for defect formation energy will represent a more energetically favorable system overall.

Chapter 3:
Results and Discussion

Once a single taggant metal atom was inserted into one of the six potential defect sites, the atoms were allowed to relax through DFT. At this stage, the base γ-UO_3 structure was expected to be fully optimized and relaxed into its most viable form. No constraints were placed on the relaxation of either the cell structure or the positions of the atoms. After repeated self-consistent iterations of the DFT calculations, the taggants resolved into their most favorable positions. The resulting structures from these calculations were analyzed based on several factors that would determine the overall favorability of each taggant and its respective defect sites. The first and most highly weighted metric for favorability is the minimized total energy of each structure. In most cases, this total energy value is used as the main quantity of comparison between structures, as a lower energy should accompany the geometric arrangement of atoms with the lowest net inter-atomic force on each atom, provided an erroneous local minimum is not found instead. For the purposes of this study, a lower minimized total energy value represents a more favorable structure overall and one most naturally likely to occur when a similar introduction of a taggant is carried out experimentally.

Though energy minimization is a useful tool for determining the viability of a candidate structure and doping site, the comparisons between minimum total energy values can only be directly compared between structures of the same taggant metal and doping style, i.e., substitutional or interstitial. This gives a useful point of comparison within these categories, as a quick calculation can give an idea of which of a set of four interstitial sites for a given metal is going to provide the best results to carry forward into further analysis. It can also be used to ensure that calculations are carried out to the conclusion of their relaxation, as these numbers are not expected to differ too highly from one to the next. Despite this usefulness, as mentioned, the energy values are only directly comparable between similar defect sites of the same metal. In order to compare between different metals or even different doping styles of the same element, the values must be corrected for the different energy inherent in the addition of a given metal into the overall system. As explained previously in section 2.3, this comparison can be simplified by introduction of the defect formation energy. The calculation of this value accounts for the energetic changes with the introduction of a given metal and other changes in the structure that come with the introduction of a defect. Once these differences are corrected for, the singular quantity of defect formation energy of each structure, metal, and defect type can be directly compared to determine overall favorability among all categories.

Beyond energetics, this study is also concerned with the impact of a given taggant on the structure of the γ-UO_3. After all, the ideal taggant will be one that has the least impact on the structure overall, as these materials are meant to be inert with respect to the nuclear fuel cycle and are only meant to act as markers for ease of tracking. To this end, other quantities were extracted and compared to those of the base γ-UO_3 structure, including lattice parameters, U-O bond distances, bond angles, as well as the bonding character of the taggants themselves with the surrounding U and O atoms. The less effect the taggant has on these various structural qualities the more attractive that taggant would be for practical applications.

Finally, the densities of states (DOS) of doped structures were considered. These plots were found to be of interest to the determination of favorable taggants and for eventual comparison to experimental work, as they can show the conducting or insulating effects of each atom in the system. Plots for each interstitial taggant are included in the respective discussions. The DOS plot of the original γ-UO_3 structure is shown in Figure 5, where it exhibits a band gap of 2.64 eV. This is overestimated compared to theoretical results by Brincat et al.[19] and experimental results by He et al.[28], at 2.40 eV and 2.38 eV respectively, however these results were obtained with a U_{eff} value of 4 eV compared to the 3 eV used in this work. The valence band goes right up to 0 eV and is dominated by the O (p) orbitals, while the conduction band is formed mainly by the U (f) orbitals.

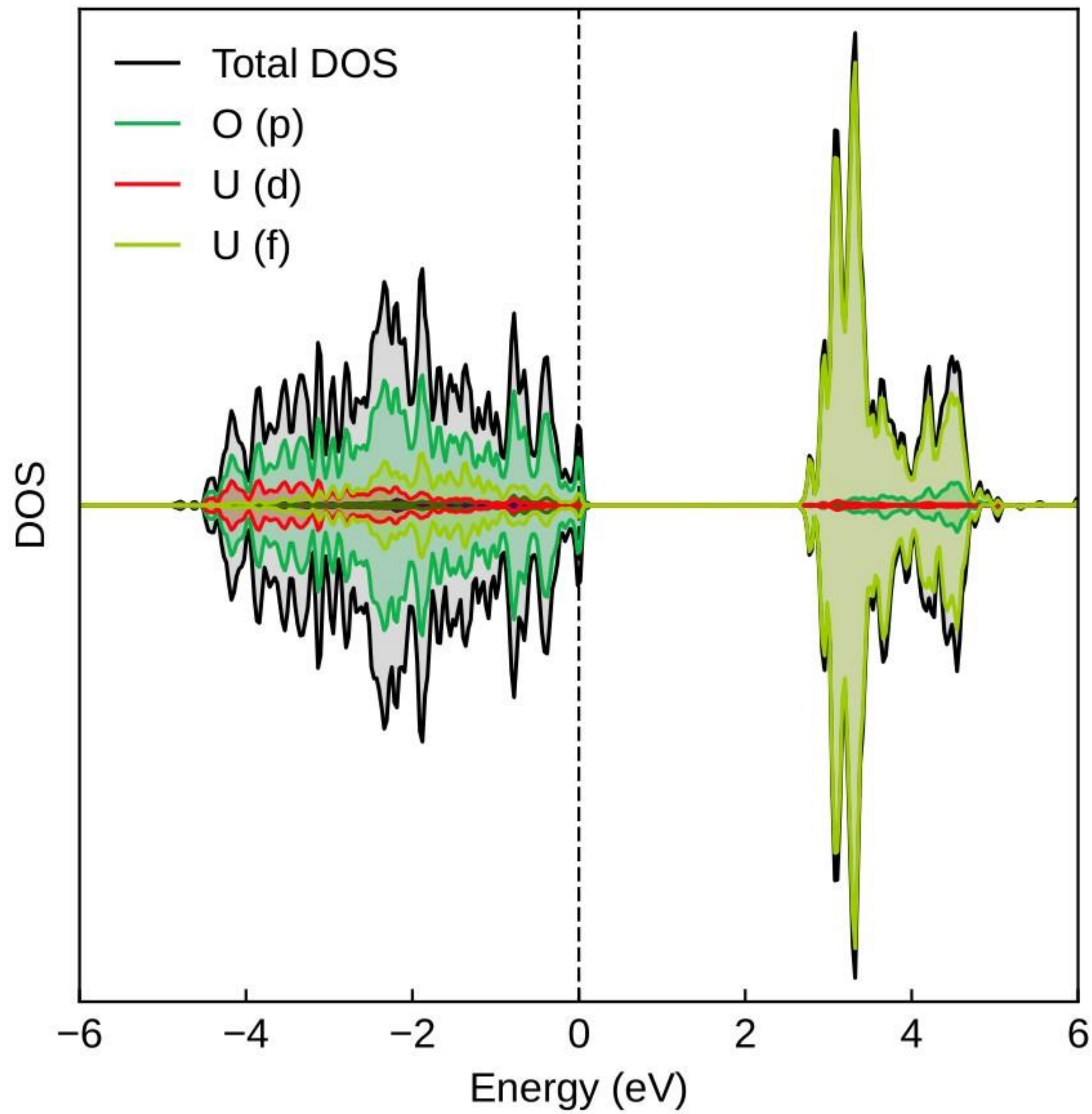

Figure 5: DOS plot for undoped tetragonal γ-UO_3

3.1 Chromium

The first taggant introduced into the γ-UO_3 system was chromium. A single Cr atom was placed one at a time into each of the six defect sites and allowed to relax through DFT. The results of these calculations were compared within each doping category to determine the most energetically favorable of the cases considered, with the results of the calculations shown in Table 2. The lattice constants and bond distances of each structure were also extracted and compared with those of the γ-UO_3 cell on its own. Reference values for lattice constants and volume can be found in the last row of Table 2, along with a percentage difference from the UO_3 cell volume in the final column. Defect formation energy calculations for Cr were carried out in several steps. First, a single-step DFT calculation was performed on a single unit cell of Cr-metal in order to find the energy inherent in adding a single atom of Cr into a given structure. In the interstitial case, this single-Cr energy was simply added to the energy of the relaxed γ-UO_3 structure, resulting in the reference value of -579.82 eV. The substitutional case was handled similarly, with the exception that the energy of the single U atom replaced by the Cr taggant atom was removed from the calculation, resulting in a reference value of -571.49 eV. These reference values were then compared to the minimized energy calculated through DFT, with the resultant defect formation energy reported in the fourth column of Table 2, able to be compared directly to the respective defect formation energy values of the other two metals.

Table 2: Cr Energetics and Lattice Constants

Chromium Doping Type	Defect Site	Total Energy (eV)	Defect Formation Energy (eV)	Lattice Constants (Å)			Volume (Å^3)	Difference in Volume (%)
				a	*b*	*c*		
Interstitial	Site *I1*	-581.40	-1.57	7.07	7.05	20.22	1007.08	2.82
	Site *I2*	-581.37	-1.55	7.02	7.05	20.33	1005.92	2.70
	Site *I3*	-581.37	-1.54	7.05	7.02	20.30	1005.63	2.67
	Site *I4*	-580.85	-1.03	6.98	7.04	20.82	1023.62	4.51
Substitutional	Site *S1*	-562.64	8.85	7.02	6.97	20.73	1014.09	3.53
	Site *S2*	-562.80	8.69	7.02	6.83	20.54	984.04	0.465
γ-UO_3	-	-570.40	-	6.96	6.96	20.21	979.49	-

Upon compilation of the total energy results and lattice constants from each of the six defect sites, a few clear trends and results emerge. Perhaps the most striking result is that the defect formation energies for each of the Cr interstitial doping sites is negative, implying an exothermic reaction occurring with the insertion of the Cr atom into the system. This is notably the only metal of the three tested that finds this result. As one of the main signifiers for favorability of a given taggant is a minimal defect formation energy, this negative result shows a strong advantage for Cr on its own. This favorability does only extend to the interstitial case, however, as in the two substitutional cases tested a much higher defect formation energy on the order of 8 eV is calculated. This begins to evince that the γ-UO_3 system shows a heavy preference for interstitial acceptance of metal taggants over substitutional. In terms of energetic favorability, the sites with the minimal energy for each defect type are Site *I1* and Site *S2* for interstitial and substitutional defects respectively. The structures and atomic positions of these two cases are displayed in Figure 6. At this point, however, it can be clearly seen that the first three interstitial sites (*I1*-*I3*) are extremely close to one another energetically, with Sites *I2* and *I3* having identical energetic results, though slightly higher than that of Site *I1*. Indeed, upon structural analysis of the atomic positions each of these three sites optimizes through DFT into the same position relative to the two periodic U sites, though located in different absolute spaces throughout the unit cell. This seems to show that this interstitial defect location is preferential to other potential locations, including that of Site *I4*. Sites *S1* and *S2* were also similar energetically, with Site *S2* having a slightly lower value and thus considered to be more favorable from this perspective.

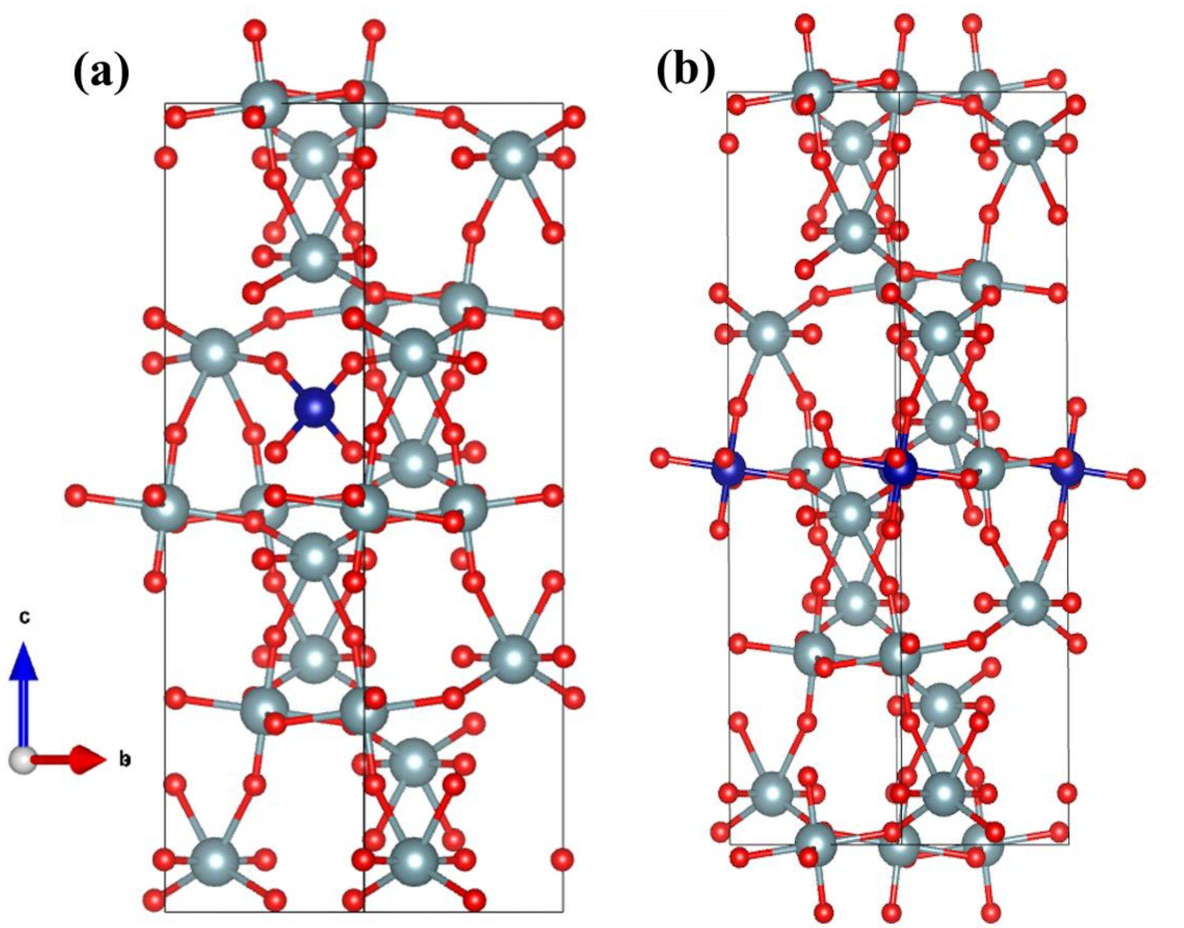

Figure 6: Most favorable Cr doped structures: (a) Interstitial Site I1 (b) Substitutional Site S2

Despite being similar energetically, each of the different doping positions did have a significant impact on the lattice constants and subsequent volume of the overall γ-UO_3 unit cell. For the interstitial defects, Sites *I1*-*I3* all had a similar impact on the volume of the unit cell, though the more energetically favorable Site *I1* did increase the volume from the base structure by about 0.1% more than Site *I2* or *I3*. Site *I4,* the least energetically favorable, did distort the ratio more, resulting in a 4% increase in volume for the unit cell overall. For the substitutional defects, there is a wider gap than between the interstitial defects, with the more favorable Site *S2* only increasing the volume of the unit cell by 0.465% compared to the original γ-UO_3 structure – by far the smallest increase among all six defect sites. Comparatively, Site *S1* seems much more in line with the effects of the interstitial defects on the overall volume of the cell, with an increase of 3.53%.

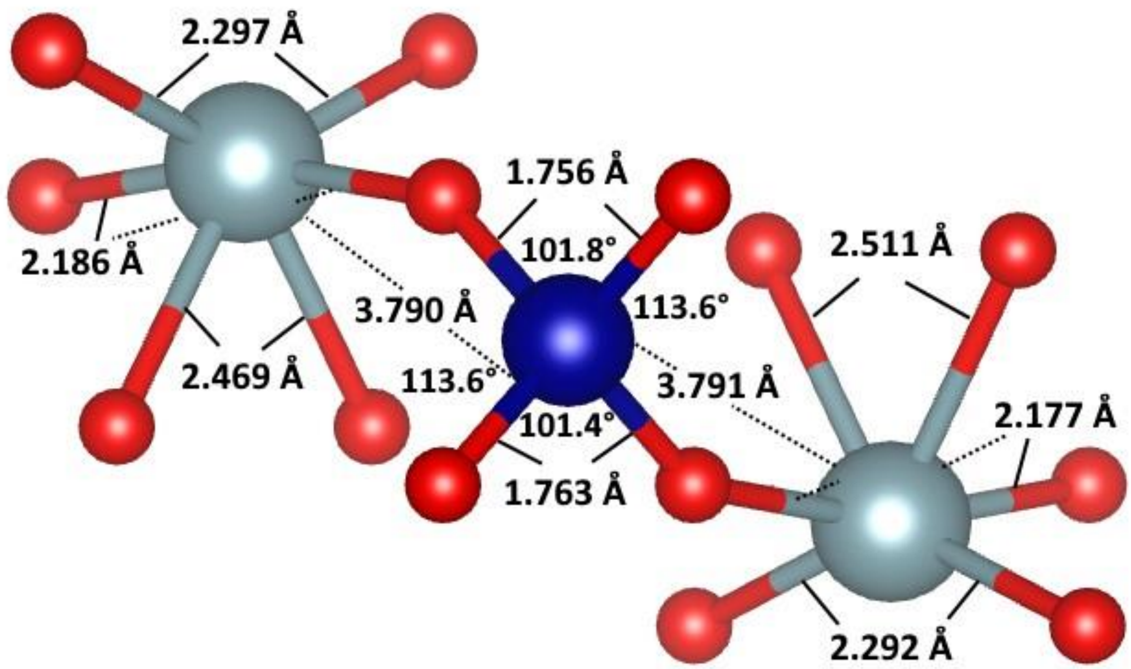

Figure 7: Nearest neighbor bond lengths and angles for Interstitial Cr Site I1

A summary of the bond lengths surrounding the doped Cr atom in *Site I1* can be seen in Figure 7. The doped atom sits equidistant between two U1 atoms with 3.79 Å separating the Cr and U. The Cr bonds tetrahedrally to four total O atoms: two with bond length of 1.756 Å and two with 1.763 Å. The bonds are also a bit distorted to be perfectly tetrahedral, with angles between bonds being 101.8°, 101.4°, and 113.6°, where the ideal tetrahedral bond would have angles closer to 109.5°. The two oxygen atoms that bridge the U and the Cr have a longer U-O bond length than similar sites in the same unit cell and those found in the original UO_3, going from 1.796 Å to 2.186 Å. Beyond these nearest neighbors, much of the unit cell remains the same as in the original γ-UO_3, showing that the metal taggant does impact the structure of its surroundings.

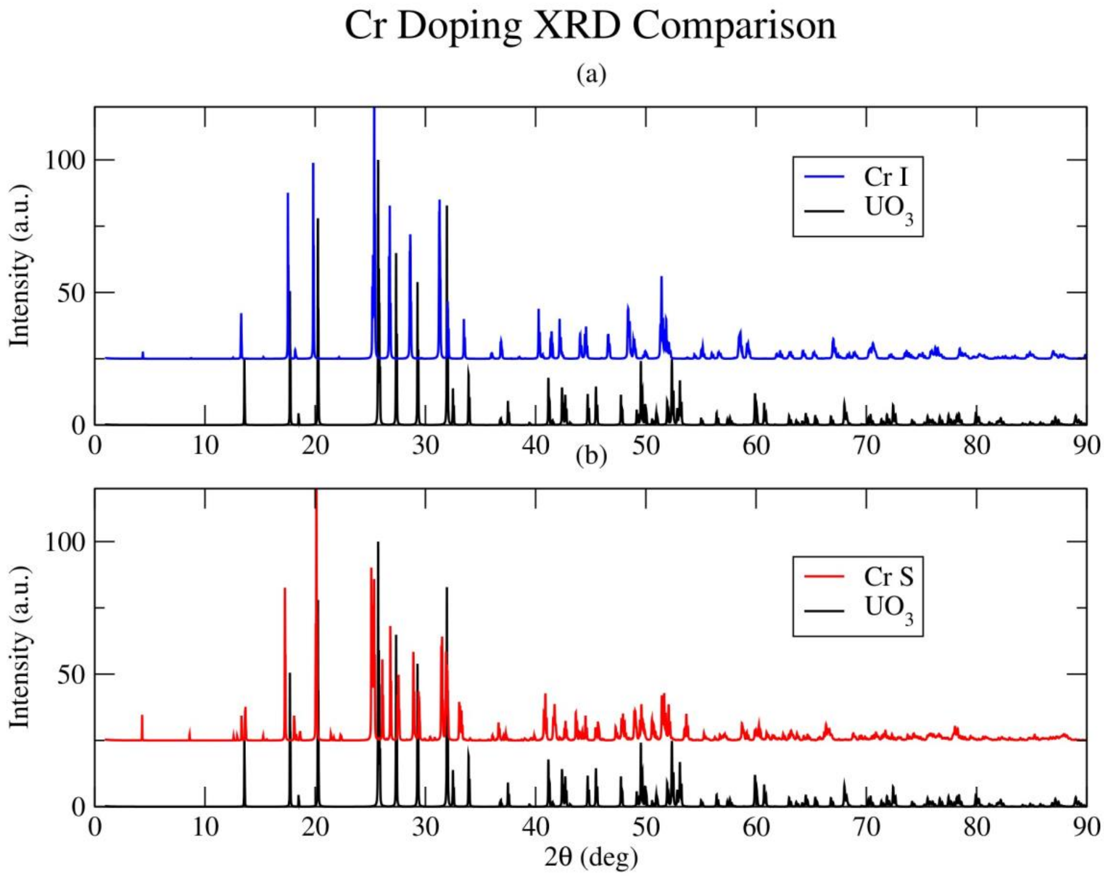

Figure 8: XRD pattern comparison for γ-UO_3 structures doped with Cr: (a) Interstitially and (b) Substitutionally

Theoretical X-ray diffraction (XRD) patterns were created for γ-UO_3 doped both interstitially and substitutionally with Cr and displayed in Figure 8. A visual comparison of these patterns with that of the base γ-UO_3 shows several differences. For the interstitial case, there is some slight peak shifting, as well as the appearance of new peaks around 5° and 42°, but otherwise the pattern remains mostly unchanged from the original. The substitutional pattern, however, shows more distortion with the addition of several new peaks where none exist in the original UO_3, especially in the clustered peaks from 25°-35° and 40°-50°.

The DOS plot for Cr interstitial doping is displayed in Figure 9. In contrast to the DOS plot for γ-UO_3 seen in Figure 5, there is no apparent band gap between the valence band and where the conduction band begins at 0 eV, with some gap states occurring due to the U (f) orbitals and Cr (d). Additional peaks for Cr (d) are seen in the conduction band, which is again dominated mostly by the U (f) orbitals.

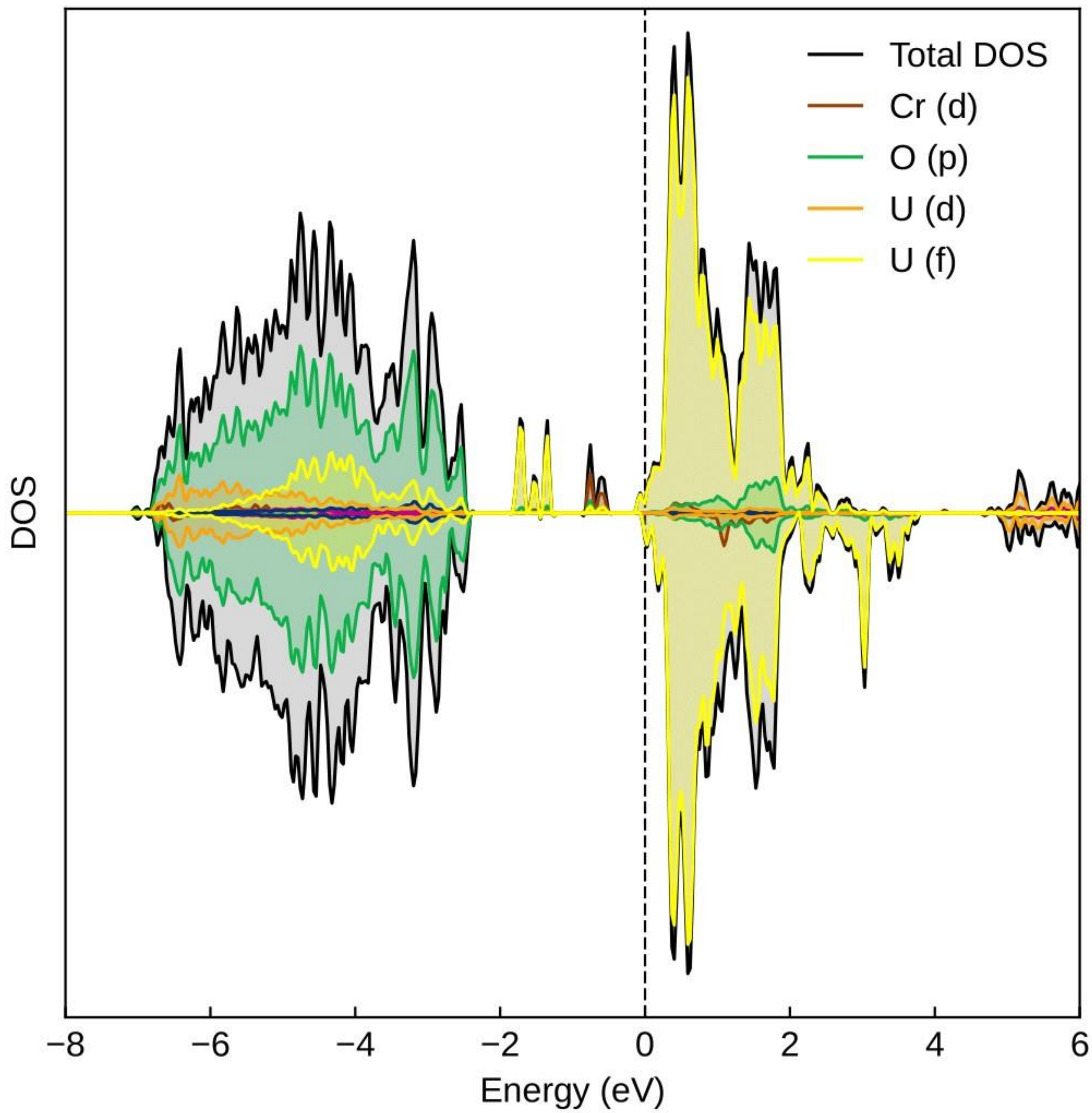

Figure 9: DOS plot for Interstitial Cr Site I1

3.2 Iron

Like the process for Cr doping, one Fe atom at a time was introduced to each of the six doping sites and optimized through DFT to its most favorable position. The energetics and lattice constants resultant from these calculations were once again compiled and displayed in Table 3, with the same reference values for the base γ-UO_3 structure displayed in the final row. Defect formation energy calculations were also carried out for the case of Fe metal atoms. Similarly to Cr, the energy for a single atom of Fe was found by performing a single-step DFT calculation of a unit cell of Fe-metal. The resultant energy was then added to that of the original γ-UO_3 structure. This is sufficient to find the formation energy reference number for the interstitial defects, in this case resulting in a value of -578.74 eV. Again, the substitutional case requires the additional step of subtracting the energy of the U atom being exchanged for the Fe atom at its original position. This provides a substitutional defect reference value of -570.41 eV. When compared with the total energy reported by the DFT calculations, a defect formation energy is found and relayed in the fourth column of Table 3. It is with the introduction of this second metal taggant that the defect formation energy value begins to best exhibit its usefulness, as now the relative energetic favorability of both Fe and Cr can be compared, despite having different absolute values for their total energies.

Table 3: Fe Energetics and Lattice Constants

Iron Doping Type	Defect Site	Total Energy (eV)	Defect Formation Energy (eV)	Lattice Constants (Å)			Volume (Å^3)	Difference in Volume (%)
				a	*b*	*c*		
Interstitial	Site *I1*	-578.58	0.159	7.02	7.01	20.46	1007.85	2.90
	Site *I2*	-578.61	0.128	7.03	7.01	20.47	1008.08	2.92
	Site *I3*	-577.09	1.64	7.07	6.95	20.92	1029.15	5.07
	Site *I4*	-577.61	1.13	7.02	7.04	20.82	1030.79	5.24
Substitutional	Site *S1*	-557.72	12.69	7.02	6.97	20.71	1014.23	3.55
	Site *S2*	-558.51	11.90	7.01	6.91	20.50	983.58	0.418
γ-UO_3	-	-570.40	-	6.96	6.96	20.21	979.49	-

With the energetic results for Fe at hand in Table 3, comparisons can begin between the various sites and defect types. For the interstitial case, Sites *I1* and *I2* have the lowest formation energies, with Site *I2* winning out with a defect formation energy about 0.03 eV lower than that of Site *I3*. Both values are very small, approaching zero, but none of the results for Fe manage to break into negative values as occurred in the Cr interstitial doping case. In another departure from the previous results, the energetics for Sites *I2* and *I3* are quite different from one another, whereas these sites were near-identical for their Cr equivalents. In fact, Site *I3* has the highest defect formation energy among the entire Fe interstitial doping catalog, even higher than the notably different Site *I4*, which proved the highest for the Cr taggant. For the substitutional defects, the trend set by Cr continues, with Site *S2* remaining the most energetically favorable. Again, a much higher defect formation energy is seen for the substitutional cases, seemingly confirming that the γ-UO_3 system has a strong preference for interstitial defects, at least for the particular taggants tested. The structures and atomic positions of the most favorable cases for the interstitial and substitutional defects, Site *I2* and Site *S2* respectively, are displayed in Figure 10.

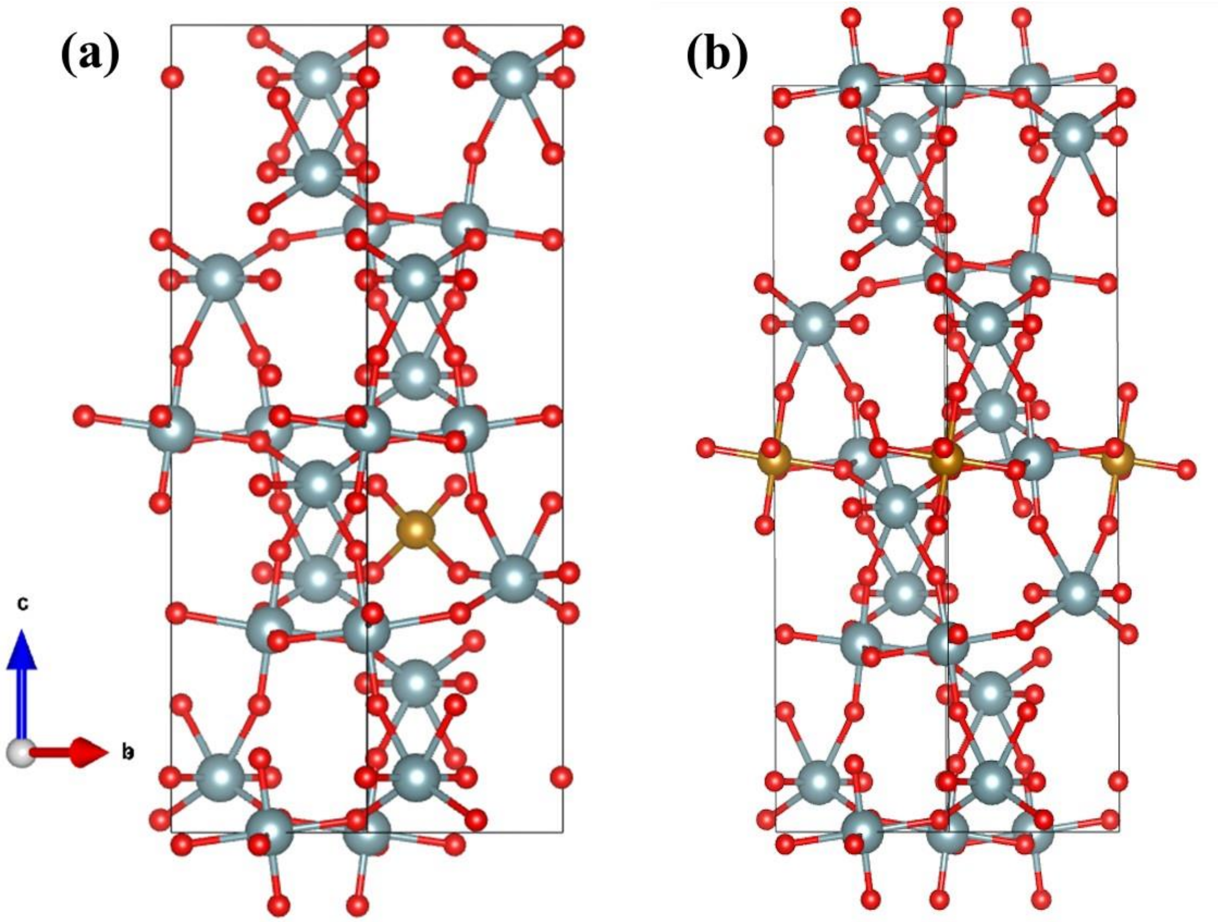

Figure 10: Most favorable Fe doped structures: (a) Interstitial Site I2 (b) Substitutional Site S2

In terms of the lattice constants, the results for Fe metal taggants show a similar trend to those of the Cr metal. In each case, an increase in the overall volume of the unit cell as compared to that of the original γ-UO_3 can be seen. As expected, Sites *I1* and *I2* show similar increases to match their energetic similarities, however again Site *I3* proves an outlier to this grouping with a percentage difference just over 2% higher. As before, however, Site *I4* continues to have the highest percentage increase in volume among all interstitial cases. The substitutional cases, too, hold the trend set by the Cr taggant, with Site *S1* having a higher increase in volume overall while Site *S2* remains much closer to the size of the original structure.

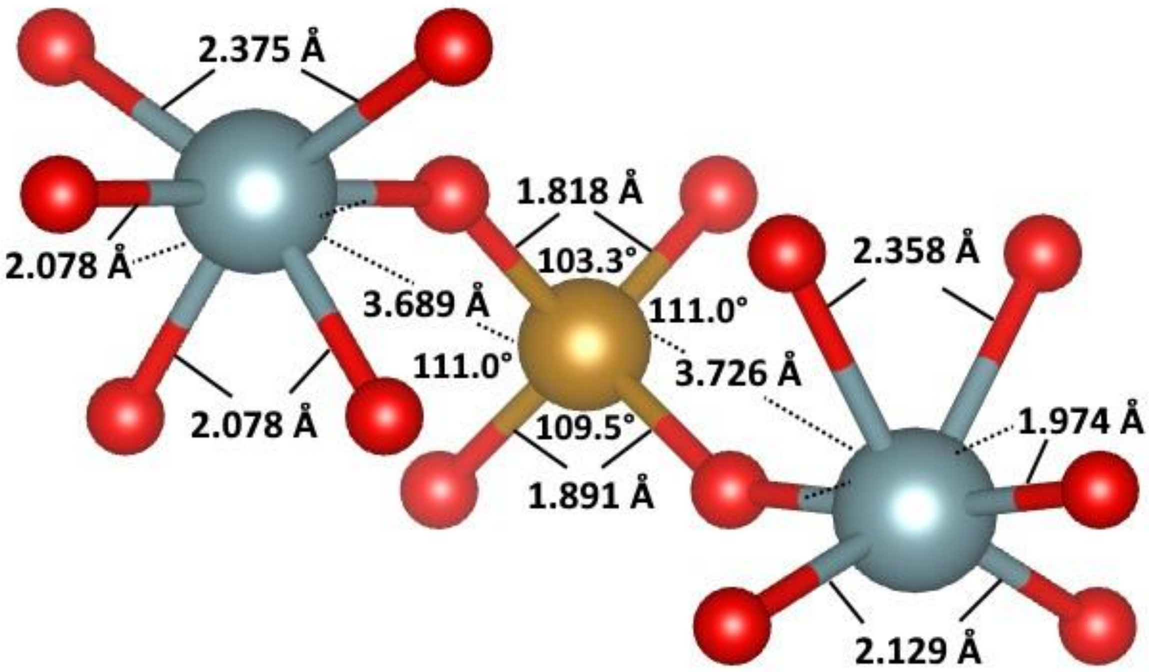

Figure 11: Nearest neighbor bond lengths and angles for Interstitial Fe Site I2

Bond lengths for Fe interstitial Site *I2* are found in Figure 11. This site is similar to the most favorable site for Cr, *I1*, but there are some differences to account for the added Fe atom. First, the doped atom is not equidistant from its two nearest neighboring U atoms, with a distance of 3.689 Å from one and 3.726 Å from the other. The Fe atom also bonds nearly tetrahedrally with four O atoms, with angles of 103.3°, 109.5°, and 111.0°. The distances between the Fe and O are longer than those between Cr and O, at 1.818 Å and 1.891 Å compared to 1.756 Å and 1.763 Å, respectively. Again, the changes in the unit cell are localized to the immediate surrounding of the Fe atom.

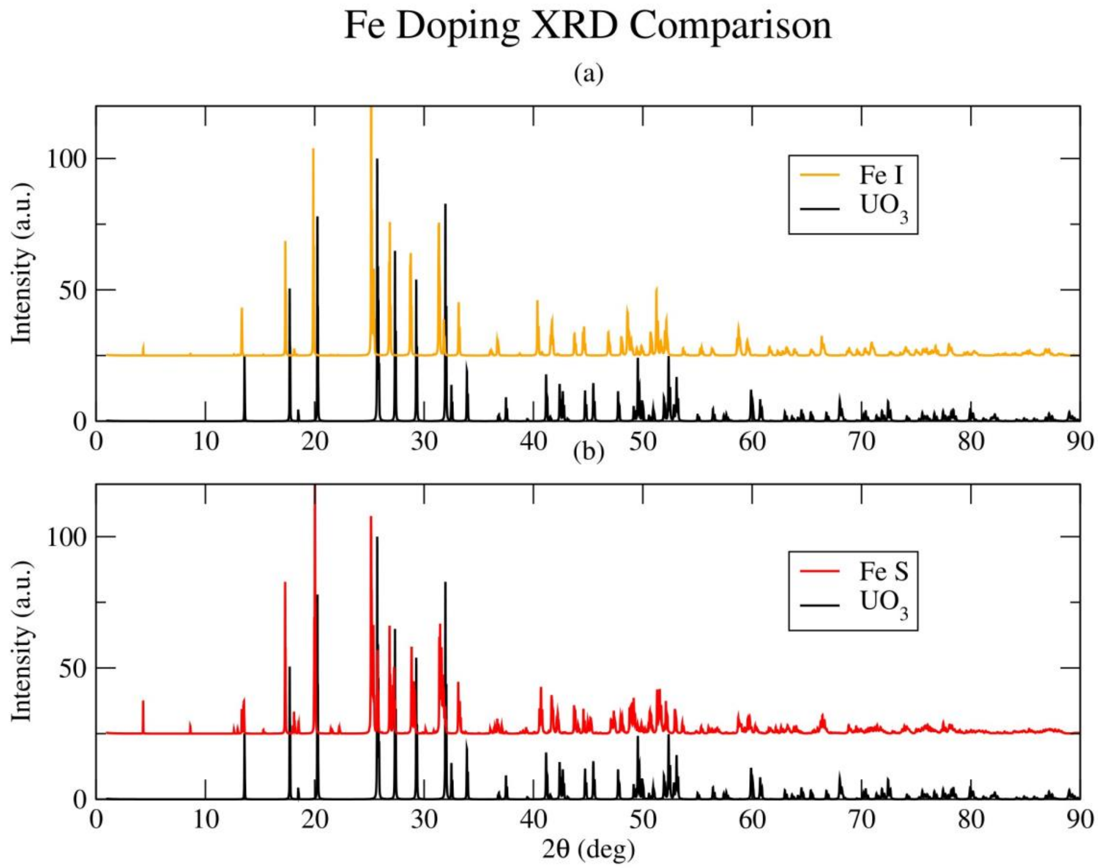

Figure 12: XRD pattern comparison for γ-UO_3 structures doped with Fe: (a) Interstitially and (b) Substitutionally

The XRD pattern for γ-UO_3 doped with Fe in Figure 12 shows similar findings to those of the Cr-doped structures. A peak begins to form near 5° in both cases, and several new peaks do appear in the substitutional case. Overall, the interstitial XRD pattern again shows the least distortion from the original UO_3 pattern.

A DOS plot for interstitial Fe can be seen in Figure 13. The contribution to the DoS from Fe is very small, with some Fe (s) contribution around the 0 eV mark. The band gap between the valence and conduction bands is 0.28 eV, with the conduction band beginning 0.65 eV past the zero line. Additional gap states are occurring between the two bands, likely distortion due to the presence of Fe.

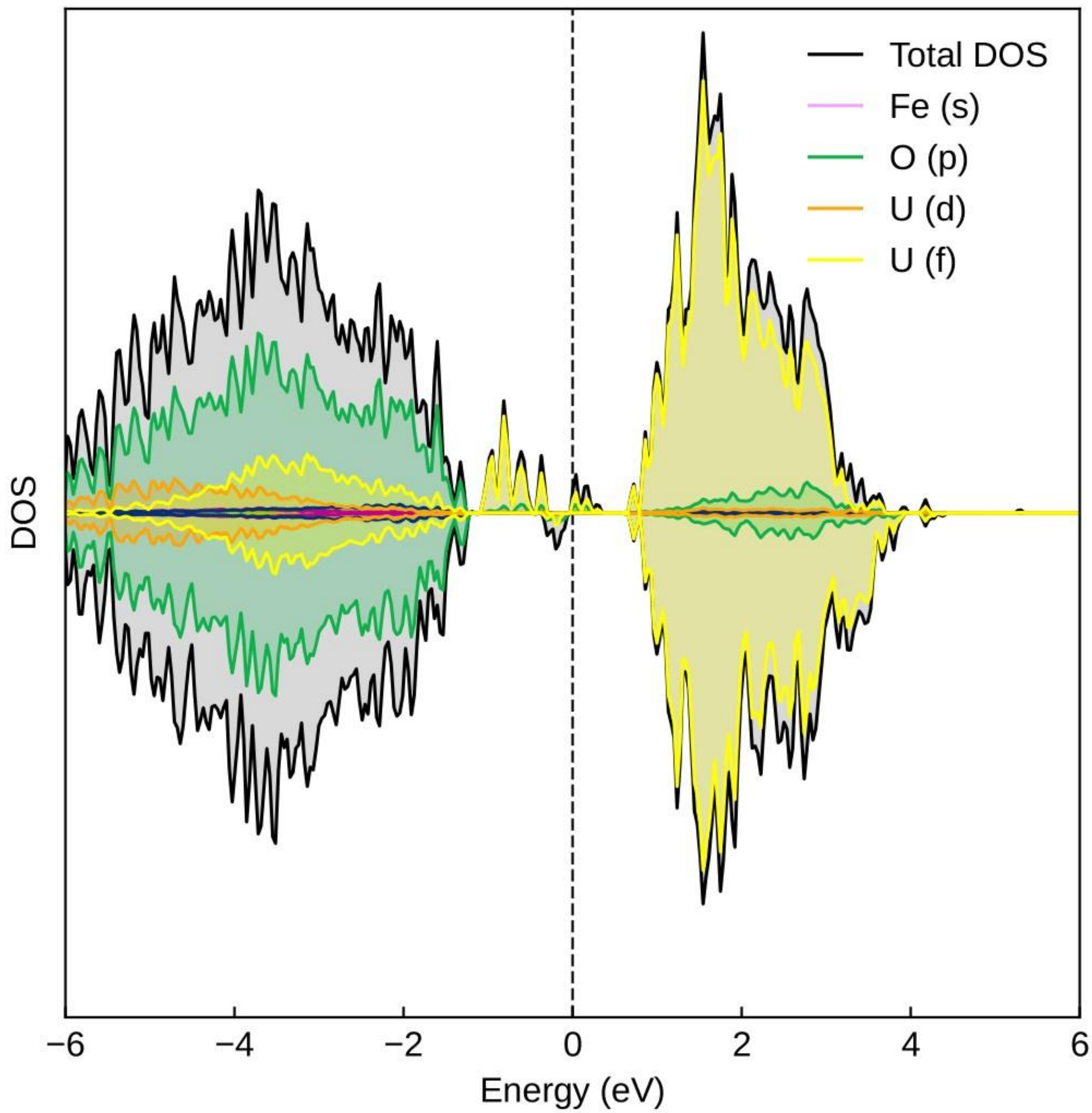

Figure 13: DOS plot for Interstitial Fe Site I2

3.3 Nickel

Finally, the taggant insertion process concluded with the addition of Ni to the γ-UO_3 cell. As in the previous cases, a single atom of Ni was introduced to six distinct doping sites, four of which were interstitial and the remaining two substitutional. Once the Ni atom was added to these sites, the entire structure was run through DFT calculations until its atomic positions and overall lattice shape reached the most favorable arrangement. Energetic and lattice constants details are reported in Table 4, which again contains in its final row the reference values for the original γ-UO_3 structure. As for all metal taggants, defect formation energy calculations were performed for ease of comparison between all structures. In this case, the energy of a single Ni atom was extracted from the single-step DFT calculation performed upon a unit cell of Ni-metal. Once added to the energy resultant from the calculation on the initial γ-UO_3, the reference value for the interstitial case was found to be -575.89 eV. The substitutional reference value was again calculated by subtraction of the energy for the single U atom being replaced by the Ni taggant, which results in a value of -567.56 eV. With these final reference values, the defect formation energies for the six Ni sites were calculated and reported in column four of Table 4. At this point, the defect formation energy values from all three metal taggants could be directly compared to one another to determine which of the metals is most energetically favorable for this system overall.

Table 4: Ni Energetics and Lattice Constants

Nickel Doping Type	Defect Site	Total Energy (eV)	Defect Formation Energy (eV)	Lattice Constants (Å)			Volume (Å^3)	Difference in Volume (%)
				a	*b*	*c*		
Interstitial	Site *I1*	-574.03	1.86	7.07	7.01	20.20	1001.37	2.23
	Site *I2*	-574.89	1.01	7.03	7.01	20.50	1010.60	3.18
	Site *I3*	-573.78	2.11	7.14	6.98	20.52	1022.68	4.41
	Site *I4*	-574.57	1.32	6.99	7.03	20.69	1016.48	3.78
Substitutional	Site *S1*	-	-	-	-	-	-	-
	Site *S2*	-553.14	14.43	7.00	6.86	20.50	984.81	0.543
γ-UO_3	-	-570.40	-	6.96	6.96	20.21	979.49	-

Before a discussion of the energetics for the Ni taggant doping, it should be mentioned that only one of the expected two substitutional defect sites was able to complete its DFT calculations. The calculations for Site *S1* attempted to run no less than six times, and in each case the system was unable to reach its relaxed state. Instead, the system began to balloon in size, and the calculations would fail. Attempts were made to try a separate instance of the same repeated U site, but similar results were found and as such no results were available for Site *S1* at the time of reporting.

Despite the omission of Site *S1*, the energetic results of the remaining five defect sites can be compared. The interstitial case for Ni was quite unlike the previous two metals. Each of the four interstitial sites has a markedly different defect formation energy, with Site *I2* ultimately having the lowest. As with the Fe metal, Site *I3* has a higher energy than Sites *I1* and *I2*, which would not have been expected from analysis of the Cr case alone. For Ni, Site *I4* has the second lowest energy, despite being the outlier in terms of actual atomic positioning. Substitutional energetics are difficult to compare with only one data point available, but the trend of substitutional defect formation energy being much higher than those of the interstitial defects does continue. Most favorable doped structures for Ni can be seen in Figure 14. It is interesting to note that the defect formation numbers across the board are the highest for Ni among all the taggants tested.

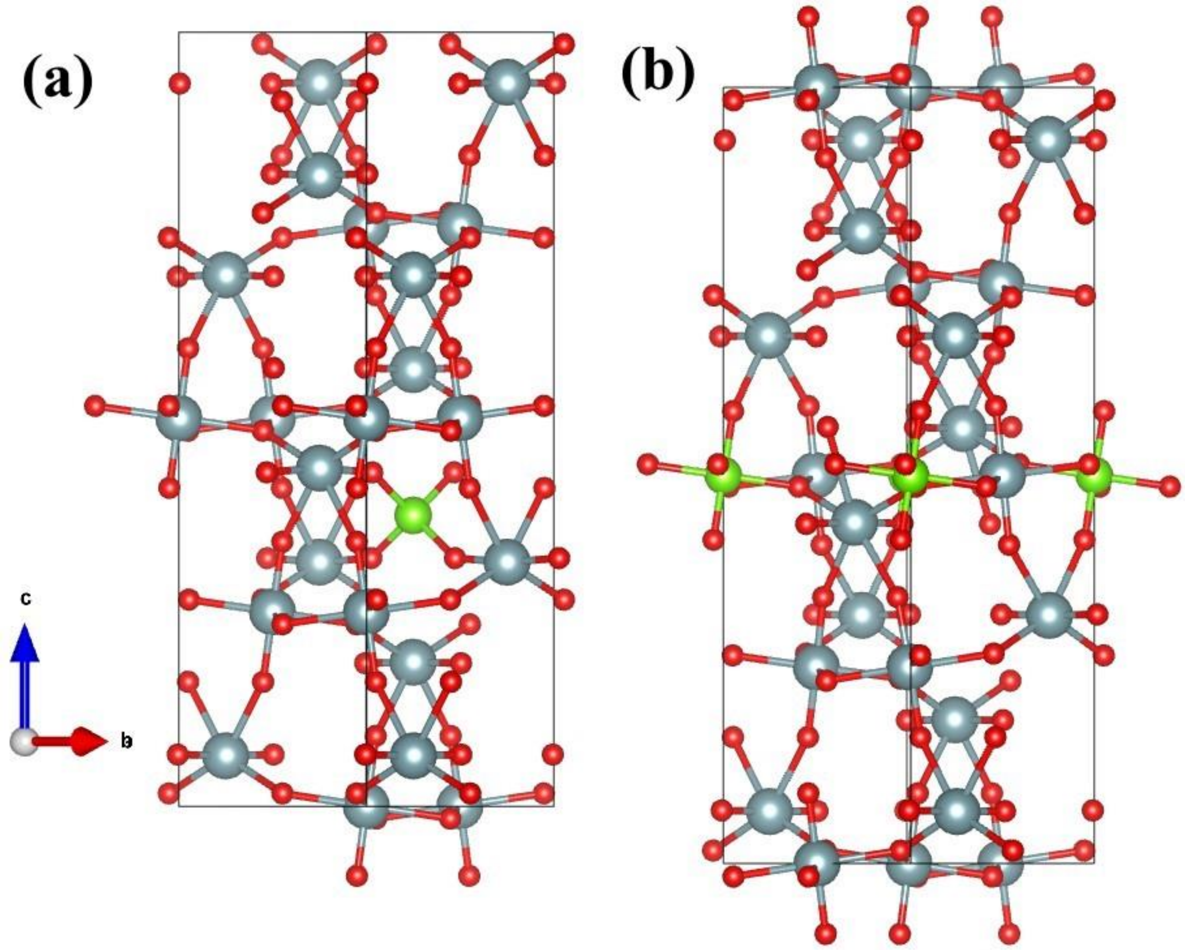

Figure 14: Most favorable Ni doped structures: (a) Interstitial Site I2 (b) Substitutional Site S2

For the lattice constants, similar results are reported as for the prior two metal taggants. In each case there is an increase in volume from that of the original γ-UO_3. These results do not appear to correlate meaningfully with the energetic favorability, as the difference in volume for Sites *I1* and *I3* is respectively lower and higher than that of the most energetically favorable Site *I2*. As seems to be the trend for each of the tested metal taggants, Site *S2* is less than one percent higher in volume as compared to the original γ-UO_3, though the value for Ni Site *S2* is the highest among the three in value.

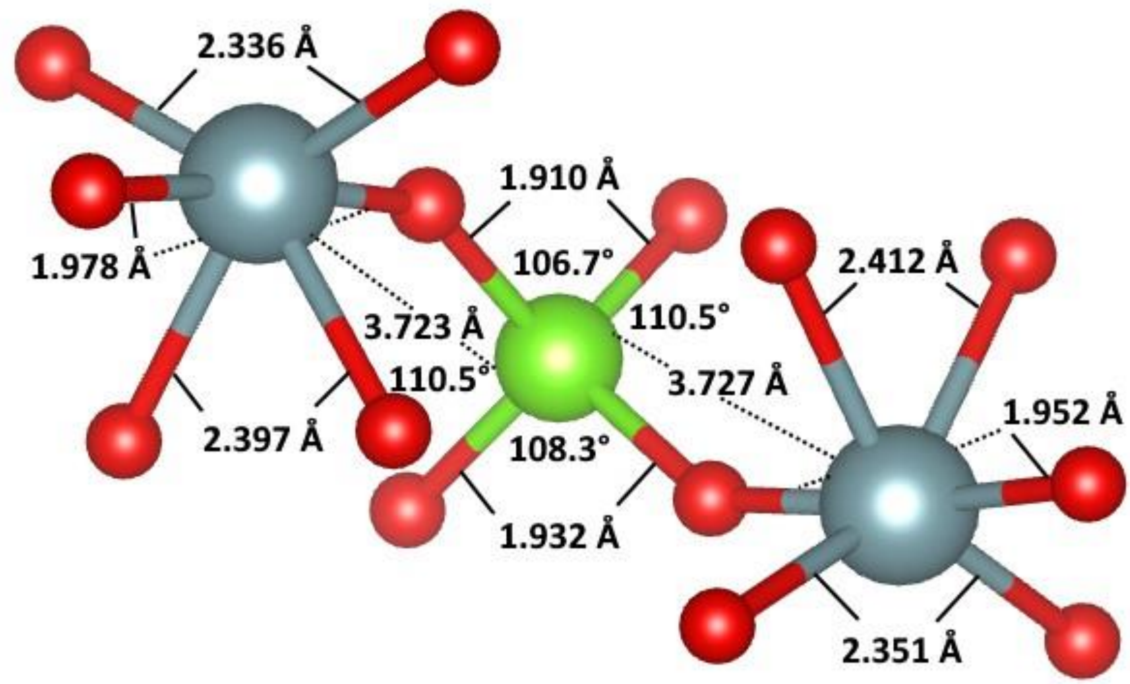

Figure 15: Nearest neighbor bond lengths and angles for Interstitial Ni Site I2

Ni bond distances are displayed in Figure 15. Like Cr, the Ni atom sits approximately equidistant from each of the two nearest U atoms. The bond lengths of the two sets of O atoms are 1.910 Å and 1.932 Å, the longest among the three sampled. The Ni atom is the closest to a tetrahedral bonded atom, with bond angles of 106.7°, 108.3°, and 110.5°, averaging closer to the ideal 109.5°. These numbers seem to correlate to the atomic number and overall size of the transition metal atom. The bond lengths of each of the U-O bonds are also affected the least from among all the doped metal structures.

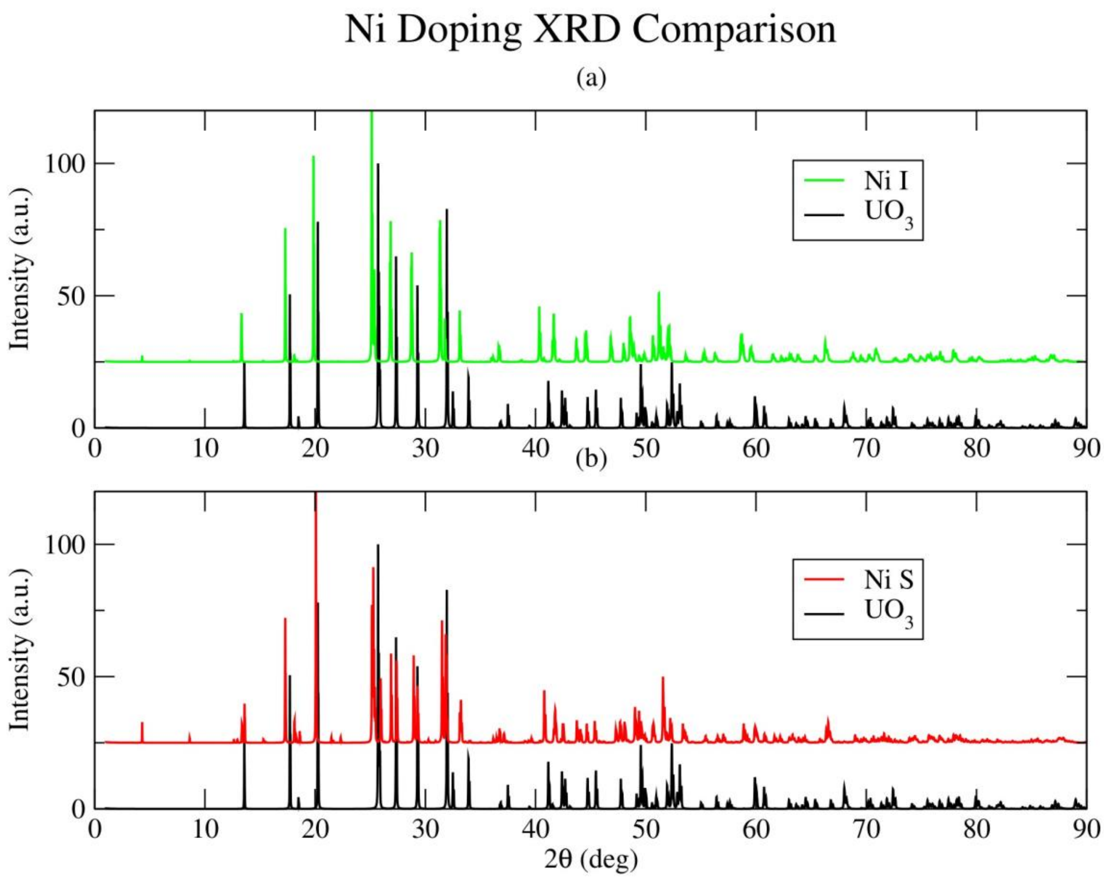

Figure 16: XRD pattern comparison for γ-UO_3 structured doped with Ni: (a) Interstitially and (b) Substitutionally

XRD patterns for Ni-doped γ-UO_3 are found in Figure 16. As with the previous two patterns, the interstitially doped Ni begins to form a peak near 5°, as well as shifting the peaks slightly from the original UO_3 positions. The substitutional case displays the same addition of extra peaks, especially between 40°-50° for Ni.

Figure 17 represents the DOS plot for interstitially doped Ni. The presence of the Ni (d) orbital contribution can be seen clearly at the tail of the valence band and around the 0 eV mark, and this plot exhibits a large band gap of 1.05 eV.

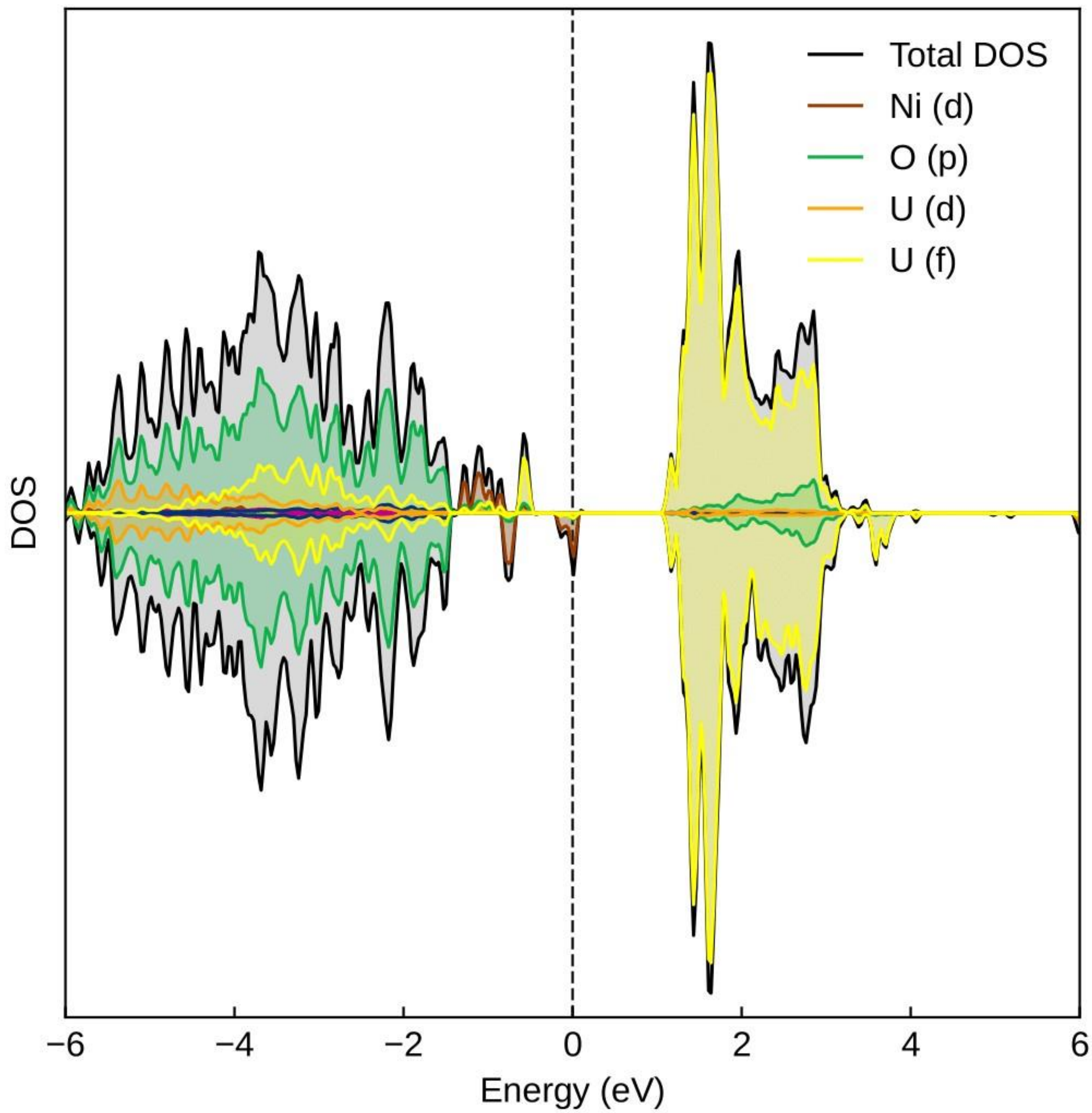

Figure 17: DOS plot for Interstitial Ni Site I2

Chapter 4:
Concluding Remarks

4.1 Overall Favorability

The results from the calculations performed on the various dopants suggest that interstitial doping is likely to be the more favorable method for taggant incorporation in γ-UO_3. Across all calculations performed the formation energies for the substitutional cases were significantly higher than those doped interstitially. The calculations also suggest Cr to be the most favorable taggant among the three tested. The formation energy associated with interstitial doping of Cr is the only one to reach negative values, all the way down to -1.57 eV, suggesting that it is an exothermic reaction and therefore likely to occur. This is compared with the most favorable formation energies of 0.128 eV and 1.01 eV for Fe and Ni, respectively. Cr also had the lowest value for change of total volume in the γ-UO_3 structures at its most favorable location compared to those of the other two metal dopants. This suggests that the introduction of Cr would have the smallest effects on the overall cell and thus would allow the use of the tagged UO_3 to continue unaffected in the nuclear fuel cycle. From these energetic and structural considerations, it seems likely that Cr doped interstitially would provide the most favorable doping strategy for a taggant in this material.

4.2 Future Work

This study presents theoretical analysis on the viability of Cr, Fe, and Ni as taggant materials in the γ-UO_3 structure. For this analysis in particular, a notable omission is the effects on the band structure of each of these metals, for which additional calculations would be required. Beyond that, it is possible that other dopants would work better as intentional forensics markers. It is also possible that other phases of UO_3 would be better hosts to these materials, as a parallel study of

β-UO_3 being carried out could show[11]. The work presented here is only a narrow window into the potential field of nuclear intentional forensics as it is being developed, and once these theoretical considerations have been exhausted a clear candidate for experimental testing can perhaps be found.

References

[1] J. Faber and G. H. Lander, "Neutron diffraction study of UO2: Antiferromagnetic state," *Phys Rev B*, vol. 14, no. 3, p. 1151, Aug. 1976, doi: 10.1103/PhysRevB.14.1151.

[2] M. A. Korotin, Z. V. Pchelkina, N. A. Skorikov, A. V. Efremov, and V. I. Anisimov, "Electronic structure of UO2.12 calculated in the coherent potential approximation taking into account strong electron correlations and spin-orbit coupling," *Physics of Metals and Metallography*, vol. 117, no. 7, pp. 655–664, Jul. 2016, doi: 10.1134/S0031918X16070103.

[3] B. Dorado, B. Amadon, M. Freyss, and M. Bertolus, "DFT+U calculations of the ground state and metastable states of uranium dioxide," *Phys Rev B Condens Matter Mater Phys*, vol. 79, no. 23, p. 235125, Jun. 2009, doi: 10.1103/PHYSREVB.79.235125/FIGURES/3/MEDIUM.

[4] Manson. Benedict, T. H. Pigford, and H. Wolfgang. Levi, *Nuclear Chemical Engineering*. McGraw-Hill Education, 1981. Accessed: Jul. 20, 2023. [Online]. Available: https://www.accessengineeringlibrary.com/content/book/9780070045316

[5] I. Sheft, S. Fried, and N. Davidson, "Preparation of Uranium Trioxide," *J Am Chem Soc*, vol. 72, no. 5, pp. 2172–2173, May 1950, doi: 10.1021/JA01161A082.

[6] M. J. Kristo, A. M. Gaffney, N. Marks, K. Knight, W. S. Cassata, and I. D. Hutcheon, "Nuclear Forensic Science: Analysis of Nuclear Material Out of Regulatory Control," *https://doi.org/10.1146/annurev-earth-060115-012309*, vol. 44, pp. 555–579, Jun. 2016, doi: 10.1146/ANNUREV-EARTH-060115-012309.

[7] S. P. LaMont *et al.*, "Use of chemical and isotopic tracers as part of an improved safeguards approach in uranium conversion facilities." pp. 111–130, Dec. 01, 2008. Accessed: Jul. 19, 2023. [Online]. Available: https://cris.bgu.ac.il/en/publications/use-of-chemical-and-isotopic-tracers-as-part-of-an-improved-safeg

[8] B. Wilson *et al.*, "Irradiation of Isotopically Tagged UO 2 Fuel for Intentional Forensics Purposes 1." [Online]. Available: http://energy.gov/downloads/doe-public-access-plan

[9] M. J. Kristo, M. Robel, and I. D. Hutcheon, "Nuclear Forensics and Attribution for Improved Energy Security: The Use of Taggants in Nuclear Fuel," Apr. 2007, doi: 10.2172/908129.

[10] A. E. Shields *et al.*, "Pressure-induced evolution of the lattice dynamics for selected UO3 polymorphs," *Journal of Nuclear Materials*, vol. 584, p. 154577, Oct. 2023, doi: 10.1016/J.JNUCMAT.2023.154577.

[11] Eduardo Montoya et al., “Beta-UO3 Study,” *Unpublished*. 2023.

[12] E. H. P. Cordfunke and P. Aling, “System UO3+ U3O8: dissociation pressure of γ-UO3,” *Transactions of the Faraday Society*, vol. 61, no. 0, pp. 50–53, Jan. 1965, doi: 10.1039/TF9656100050.

[13] B. O. Loopstra, J. C. Taylor, and A. B. Waugh, “Neutron powder profile studies of the gamma uranium trioxide phases,” *J Solid State Chem*, vol. 20, no. 1, pp. 9–19, Jan. 1977, doi: 10.1016/0022-4596(77)90046-9.

[14] G. Kresse and J. Furthmüller, “Efficient iterative schemes for *ab initio* total-energy calculations using a plane-wave basis set,” *Phys Rev B*, vol. 54, no. 16, p. 11169, Oct. 1996, doi: 10.1103/PhysRevB.54.11169.

[15] G. Kresse and J. Hafner, “*Ab initio* molecular dynamics for liquid metals,” *Phys Rev B*, vol. 47, no. 1, p. 558, Jan. 1993, doi: 10.1103/PhysRevB.47.558.

[16] G. Kresse and J. Furthmiiller B ’, “Efficiency of ab-initio total energy calculations for metals and semiconductors using a plane-wave basis set,” 1996.

[17] G. Kresse and D. Joubert, “From ultrasoft pseudopotentials to the projector augmented-wave method,” *Phys Rev B*, vol. 59, no. 3, p. 1758, Jan. 1999, doi: 10.1103/PhysRevB.59.1758.

[18] J. P. Perdew, K. Burke, and M. Ernzerhof, “Generalized Gradient Approximation Made Simple,” *Phys Rev Lett*, vol. 77, no. 18, p. 3865, Oct. 1996, doi: 10.1103/PhysRevLett.77.3865.

[19] N. A. Brincat, S. C. Parker, M. Molinari, G. C. Allen, and M. T. Storr, “Ab initio investigation of the UO3 polymorphs: Structural properties and thermodynamic stability,” *Inorg Chem*, vol. 53, no. 23, pp. 12253–12264, Dec. 2014, doi: 10.1021/IC500791M/SUPPL_FILE/IC500791M_SI_001.PDF.

[20] S. L. Dudarev, G. A. Botton, S. Y. Savrasov, C. J. Humphreys, and A. P. Sutton, “Electron-energy-loss spectra and the structural stability of nickel oxide: An LSDA+U study,” *Phys Rev B*, vol. 57, no. 3, p. 1505, Jan. 1998, doi: 10.1103/PhysRevB.57.1505.

[21] T. P. Kaloni, N. Onder, J. Pencer, and E. Torres, “DFT+U approach on the electronic and thermal properties of hypostoichiometric UO2,” *Ann Nucl Energy*, vol. 144, p. 107511, Sep. 2020, doi: 10.1016/J.ANUCENE.2020.107511.

[22] E. Torres and T. P. Kaloni, “Thermal conductivity and diffusion mechanisms of noble gases in uranium dioxide: A DFTþU study,” 2019, doi: 10.1016/j.jnucmat.2019.04.040.

[23] P. F. Weck, E. Kim, C. F. Jové-Colón, and D. C. Sassani, “On the role of strong electron correlations in the surface properties and chemistry of uranium dioxide,”

Dalton Transactions, vol. 42, no. 13, pp. 4570–4578, Mar. 2013, doi: 10.1039/C3DT32536A.

[24] K. Momma and F. Izumi, “VESTA 3 for three-dimensional visualization of crystal, volumetric and morphology data,” *urn:issn:0021-8898*, vol. 44, no. 6, pp. 1272–1276, Oct. 2011, doi: 10.1107/S0021889811038970.

[25] P. Turner, “XMGRACE.” Center for Coastal and Land-Margin Research, Oregon Graduate Institute of Science and Technology, Beaverton, OR, 2005.

[26] A. M Ganose, A. J Jackson, and D. O Scanlon, “sumo: Command-line tools for plotting and analysis of periodic ab initio calculations,” *J Open Source Softw*, vol. 3, no. 28, p. 717, Aug. 2018, doi: 10.21105/JOSS.00717.

[27] A. Togo and I. Tanaka, “First principles phonon calculations in materials science,” 2015, doi: 10.1016/j.scriptamat.2015.07.021.

[28] H. He, D. A. Andersson, D. D. Allred, and K. D. Rector, “Determination of the insulation gap of uranium oxides by spectroscopic ellipsometry and density functional theory,” *Journal of Physical Chemistry C*, vol. 117, no. 32, pp. 16540–16551, Aug. 2013, doi: 10.1021/JP401149M/ASSET/IMAGES/LARGE/JP-2013-01149M_0007.JPEG.

Curriculum Vita

Nicholas James Wilson earned a bachelor's degree in physics from the University of Nevada – Las Vegas in December 2020, graduating Magna Cum Laude from the Honors College. His interest in applications of density functional theory led him to continue his studies at the University of Texas at El Paso where he is working toward a master's degree, also in physics. He will be the first graduate student from the CMREE group under Dr. Eunja Kim, with whom he has been working since June 2020. During his time at UTEP, Nick attended several conferences and participated in two separate research endeavors. After completing his master's degree, Nick will be applying his physics skills in the field as a Nuclear Material Control & Accountability Scientist at Nevada National Security Site outside Las Vegas.

Contact: Nicholas.J.Wilson.11@gmail.com